Check for updates

The CNS Myelin Proteome: Deep Profile and Persistence After Post-mortem Delay

Olaf Jahn[1], Sophie B. Siems[2], Kathrin Kusch[2], Dörte Hesse[1], Ramona B. Jung[2], Thomas Liepold[1], Marina Uecker[1], Ting Sun[2] and Hauke B. Werner[2]*

[1] Proteomics Group, Max Planck Institute of Experimental Medicine, Göttingen, Germany, [2] Department of Neurogenetics, Max Planck Institute of Experimental Medicine, Göttingen, Germany

Myelin membranes are dominated by lipids while the complexity of their protein composition has long been considered to be low. However, numerous additional myelin proteins have been identified since. Here we revisit the proteome of myelin biochemically purified from the brains of healthy c56Bl/6N-mice utilizing complementary proteomic approaches for deep qualitative and quantitative coverage. By gel-free, label-free mass spectrometry, the most abundant myelin proteins PLP, MBP, CNP, and MOG constitute 38, 30, 5, and 1% of the total myelin protein, respectively. The relative abundance of myelin proteins displays a dynamic range of over four orders of magnitude, implying that PLP and MBP have overshadowed less abundant myelin constituents in initial gel-based approaches. By comparisons with published datasets we evaluate to which degree the CNS myelin proteome correlates with the mRNA and protein abundance profiles of myelin and oligodendrocytes. Notably, the myelin proteome displays only minor changes if assessed after a post-mortem delay of 6 h. These data provide the most comprehensive proteome resource of CNS myelin so far and a basis for addressing proteomic heterogeneity of myelin in mouse models and human patients with white matter disorders.

Keywords: oligodendrocyte, myelin proteome, central nervous system (CNS), demyelination, post-mortem delay, autopsy, label-free proteomics, transcriptome

INTRODUCTION

In the central nervous system (CNS) of vertebrates, the velocity of nerve conduction is accelerated by the insulation of axons with multiple layers of myelin membrane provided by oligodendrocytes (Nave and Werner, 2014; Snaidero and Simons, 2017). Compared to other cellular membranes myelin is unusually enriched for lipids, in particular cholesterol, galactolipids and plasmalogens (Norton and Poduslo, 1973a; Schmitt et al., 2015; Poitelon et al., 2020). Indeed, the biogenesis of myelin may involve the coalescence of lipid-rich membrane-microdomains in the oligodendroglial secretory pathway (Lee, 2001; Chrast et al., 2011). Notably, the dominant CNS myelin protein, proteolipid protein (PLP), displays a high affinity to cholesterol-rich membrane-microdomains (Simons et al., 2000; Werner et al., 2013). PLP and other cholesterol-associated myelin proteins may thus enhance the coalescence and intracellular traffic of prospective myelin membranes (Schardt et al., 2009). Indeed, both cholesterol and PLP are rate-limiting for myelination, as demonstrated

by the dysmyelination observed in mice lacking oligodendroglial cholesterol synthesis (Saher et al., 2005) or PLP-expression (Yool et al., 2001; Möbius et al., 2008; de Monasterio-Schrader et al., 2013).

As a key stage of myelination, the compaction of adjacent CNS myelin layers requires myelin basic protein (MBP), as evidenced by the complete lack of compact myelin in the CNS of MBP-deficient *shiverer*-mice (Roach et al., 1985). It is now thought that MBP both displaces filamentous actin and cytoskeleton-associated proteins (Nawaz et al., 2015; Zuchero et al., 2015; Snaidero et al., 2017) and saturates negative charges of the headgroups of phosphatidylinositol-4,5-bisphosphate (PIP$_2$) on the cytoplasmic myelin membrane surfaces (Musse et al., 2008; Nawaz et al., 2009, 2013) thereby pulling together and compacting myelin membranes at the major dense line (Raasakka et al., 2017).

It has been noted already in the early 1970s that PLP and MBP constitute the most abundant CNS myelin proteins. At that time the methods were developed for the enrichment of myelin from nervous tissue by sucrose density gradient centrifugation (Norton and Poduslo, 1973b; Erwig et al., 2019a) separation by one-dimensional (1D)-polyacrylamide gel electrophoresis (SDS-PAGE) and protein staining using Buffalo Black (Morris et al., 1971) Fast Green (Morell et al., 1972) or Coomassie Blue (Magno-Sumbilla and Campagnoni, 1977). Indeed, only few bands were visible that we now know are mainly constituted by PLP, MBP and cyclic nucleotide phosphodiesterase (CNP; Sprinkle et al., 1983). Deficiency of CNP in mice impairs both the ultrastructure of myelin and the long-term preservation of axonal integrity (Lappe-Siefke et al., 2003; Edgar et al., 2009; Patzig et al., 2016; Snaidero et al., 2017).

Evidently, the protein composition of myelin is more complex when considering that various additional myelin proteins have been identified, including myelin associated glycoprotein (MAG; Quarles, 2007; Myllykoski et al., 2018), myelin oligodendrocyte glycoprotein (MOG; Johns and Bernard, 1999; von Büdingen et al., 2015), and claudin 11 (CLDN11; Gow et al., 1999; Denninger et al., 2015). This insight motivated attempts to utilize the emerging mass spectrometric techniques to approach all myelin proteins at once, thereby covering the entire myelin proteome. Indeed, purified myelin is suited for systematic assessment of its molecular constituents (De Monasterio-Schrader et al., 2012; Gopalakrishnan et al., 2013). Most early approaches involved 2D-gels (Taylor et al., 2004; Vanrobaeys et al., 2005; Werner et al., 2007), soon to be complemented by gel-free shotgun-approaches (Vanrobaeys et al., 2005; Roth et al., 2006; Dhaunchak et al., 2010) and hybrid workflows (Ishii et al., 2009). However, first systematic information on the relative abundance of myelin proteins was achieved by label-free quantification involving peptide-separation by liquid chromatography (LC) coupled to detection with quadrupole time-of-flight (QTOF) mass spectrometery (MS) (Jahn et al., 2009) or by chemical peptide labeling with isobaric tags for relative and absolute quantitation (iTRAQ) and subsequent LC-MS-analysis (Manrique-Hoyos et al., 2012). A meta-analysis of the approaches to the myelin proteome published by 2012

is available (De Monasterio-Schrader et al., 2012). Since then, label-free protein quantification by LC-MS has proven useful in the differential analysis of myelin in mouse models including mice lacking PLP, CNP, or MAG (Patzig et al., 2016). For example, this approach allowed identifying cytoskeletal septin filaments to stabilize the ultrastructure of CNS myelin, thereby preventing the formation of pathological myelin outfoldings (Patzig et al., 2016; Erwig et al., 2019b).

The intention of this work was to both establish an updated comprehensive compendium of the proteins associated with CNS myelin and to accurately quantify their relative abundance, as recently achieved for the proteome of myelin in the peripheral nervous system (Siems et al., 2020). To this aim we combined various gel-based and gel-free proteomic techniques. In particular, we used nano-flow ultra-performance liquid chromatography (nanoUPLC) for peptide separation and an ion mobility-enabled QTOF-system for label-free protein quantification by data-independent acquisition (DIA) mass spectrometry in an alternating low and elevated energy mode (MS^E). While the MS^E-mode allows quantifying myelin proteins with the required dynamic range of over four orders of magnitude, an ion mobility-enhanced version thereof [referred to as ultra-definition (UD)-MS^E] covers about twice as many myelin-associated proteins, though at the expense of dynamic range. Our workflow thus facilitates both to reliably quantify the exceptionally abundant PLP, MBP, and CNP and to appreciate the complexity of low-abundant myelin constituents.

MATERIALS AND METHODS

Animals
Male c57BL/6N wild-type mice at postnatal day 75 (P75) were used for all experiments except for the differential analysis of myelin purified from brains immediately frozen after dissection compared to a post-mortem delay of 6 h at room temperature (**Figure 4**), for which female c57BL/6N wild-type mice at P56 were used. Mice were bred and kept in the animal facility of the Max Planck Institute of Experimental Medicine and sacrificed by cervical dislocation. For the procedure of sacrificing mice for subsequent preparation of tissue, all regulations given in the German animal protection law (TierSchG §4) are followed. Since sacrificing of rodents is not an experiment on animals according to §7 Abs. 2 Satz 3 TierSchG, no specific authorization or notification is required for the present work.

Myelin Purification
A myelin-enriched light-weight membrane fraction was biochemically purified from mouse brains by sucrose density centrifugation and osmotic shocks as recently described in detail (Erwig et al., 2019a). Mice were sacrificed by cervical dislocation at the indicated ages as three biological replicates per condition ($n = 3$). Protein concentration was determined using the DC Protein Assay Kit (Bio-Rad). Initial quality control by gel electrophoresis and silver staining of gels was performed as described (de Monasterio-Schrader et al., 2013; Joseph et al., 2019). Briefly, samples were separated on a 12% SDS-PAGE gel

(1 h at 200 V) using the Bio-Rad system, fixated overnight in 10% [v/v] acetic acid and 40% [v/v] ethanol and then washed in 30% ethanol (2 × 20 min) and ddH$_2$O (1 × 20 min). For sensitization, gels were incubated 1 min in 0.012% [v/v] Na$_2$S$_2$O$_3$ and subsequently washed with ddH$_2$O (3 × 20 s). For silver staining, gels were impregnated for 20 min in 0.2% [w/v] AgNO$_3$/0.04% formaldehyde, washed with ddH$_2$O (3 × 20 s) and developed in 3% [w/v] Na$_2$CO$_3$/0.04% [w/v] formaldehyde. The reaction was stopped by exchanging the solution with 5% [v/v] acetic acid.

Gel-Based Proteome Analysis of Myelin

Gel-electrophoretic separation of myelin proteins with different pre-cast gel systems (Serva) was performed essentially as recently described in detail (Erwig et al., 2019a). Briefly, 1D separations were performed with 5 μg protein load before (pre-wash) or after (post-wash) subjecting myelin to consecutive high-salt and high-pH washing/centrifugation cycles as previously described (Werner et al., 2007; Jahn et al., 2013). Automated tryptic in-gel digestion of proteins in gel bands (Schmidt et al., 2013) and protein identification by LC-MS was performed as described (Ott et al., 2015). For 2D separations, myelin was first delipidated by methanol/chloroform precipitation and 300 μg protein was loaded on a 24 cm immobilized non-linear pH-gradient 3-12 strip (Serva) by active rehydration (Erwig et al., 2019a). Automated tryptic in-gel digestion of proteins in gel spots and protein identification by MALDI-TOF mass spectrometry was performed as described (Jahn et al., 2006; Werner et al., 2007).

Label-Free Quantification of Myelin Proteins

In-solution digestion of myelin proteins according to an automated filter-aided sample preparation (FASP) protocol (Erwig et al., 2019a) and LC-MS-analysis by different MS^E-type data-independent acquisition (DIA) mass spectrometry approaches was performed as recently established for PNS myelin (Siems et al., 2020). Briefly, protein fractions corresponding to 10 μg myelin protein were dissolved in lysis buffer (1% ASB-14, 7 M urea, 2 M thiourea, 10 mM DTT, 0.1 M Tris pH 8.5) and processed according to a CHAPS-based FASP protocol in centrifugal filter units (30 kDa MWCO, Merck Millipore). After removal of the detergents, protein alkylation with iodoacetamide, and buffer exchange to digestion buffer [50 mM ammonium bicarbonate (ABC), 10% acetonitrile], proteins were digested overnight at 37°C with 400 ng trypsin. Tryptic peptides were recovered by centrifugation and extracted with 40 μl of 50 mM ABC and 40 μl of 1% trifluoroacetic acid (TFA), respectively. Combined flow-through were directly subjected to LC-MS-analysis. For quantification according to the TOP3 approach (Silva et al., 2006), aliquots were spiked with 10 fmol/μl of yeast enolase-1 tryptic digest or Hi3 EColi standard (Waters Corporation), the latter containing a set of quantified synthetic peptides derived from E. coli. Chaperone protein ClpB.

Nanoscale reversed-phase UPLC separation of tryptic peptides was performed with a nanoAcquity UPLC system equipped with a Symmetry C18 5 μm, 180 μm × 20 mm trap column and a HSS T3 C18 1.8 μm, 75 μm × 250 mm analytical column (Waters Corporation) maintained at 45°C. Peptides were separated over 120 min at a flow rate of 300 nl/min with a gradient comprising two linear steps of 3–35% mobile phase B (acetonitrile containing 0.1% formic acid) in 105 min and 35–60% mobile phase B in 15 min, respectively. Mass spectrometric analysis of tryptic peptides was performed using a Synapt G2-S QTOF mass spectrometer equipped with ion mobility option (Waters Corporation). UDMS^E analysis was performed in the ion mobility-enhanced data-independent acquisition mode with drift time-specific collision energies as described in detail (Distler et al., 2014a, 2016). Continuum LC-MS data were processed using Waters ProteinLynx Global Server (PLGS) and searched against a custom database compiled by adding the sequence information for yeast enolase 1, E. coli Chaperone protein ClpB and porcine trypsin to the UniProtKB/Swiss-Prot mouse proteome and by appending the reversed sequence of each entry to enable the determination of false discovery rate (FDR). Precursor and fragment ion mass tolerances were automatically determined by PLGS and were typically below 5 ppm for precursor ions and below 10 ppm (root mean square) for fragment ions. Carbamidomethylation of cysteine was specified as fixed and oxidation of methionine as variable modification. One missed trypsin cleavage was allowed. Minimal ion matching requirements were two fragments per peptide, five fragments per protein, and one peptide per protein. The FDR for protein identification was set to 1% threshold.

For post-identification analysis including TOP3 quantification of proteins, the freely available software ISOQuant[1] was used (Kuharev et al., 2015). Only peptides with a minimum length of seven amino acids that were identified with scores above or equal to 5.5 in at least two runs were considered. FDR for both peptides and proteins was set to 1% threshold and only proteins reported by at least two peptides (one of which unique) were quantified as parts per million (ppm) abundance values (i.e., the relative amount (w/w) of each protein in respect to the sum over all detected proteins). The Bioconductor R packages "limma" and "q-value" were used to detect significant changes in protein abundance by moderated t-statistics as described (Ambrozkiewicz et al., 2018; Siems et al., 2020). For proteome profiling of wild-type myelin by MS^E and UDMS^E, three independent experiments were performed, each with three biological replicates and sample processing with duplicate digestion and injection, resulting in a total of 12 LC-MS runs per experiment. Abundance values in ppm are given as averages of the four technical replicates per biological replicate and only proteins quantified in at least two out of three experiments are reported in the proteome resource (**Supplementary Table S1**). Proteins identified as contaminants from blood (albumin, hemoglobin) or hair cells (keratins) were removed from the list. Proteome profiling comparing wild-type myelin without and with post-mortem delay (**Figure 4** and **Supplementary Table S2**) was performed with three biological replicates and duplicate digestion, resulting in a total of 6 LC-MS runs per condition. Data acquisition was performed in the DRE-UDMS^E mode

---

[1]www.isoquant.net

(Siems et al., 2020) i.e., a deflection device was cycled between full (100% for 0.4 s) and reduced (5% for 0.4 s) ion transmission during one 0.8 s full scan, thereby providing a compromise between identification rates and dynamic range.

Interpretation of Single-Cell Resolution Transcriptome Data

Published single-cell RNA-sequencing (scRNA-seq) gene expression matrices from datasets GSE60361 (Zeisel et al., 2015), GSE75330 (Marques et al., 2016), and GSE113973 (Falcão et al., 2018), were obtained from Gene Expression Omnibus (GEO) and analyzed using R package Seurat v3.1.0 (Butler et al., 2018; Stuart et al., 2019). Mature oligodendrocyte cell populations were selected from each dataset as specified in the results section and normalized gene counts were used for calculating average expression profiles across single cells. Bulk proteome and transcriptome datasets specified in the results section were used as supplied in the **Supplementary Tables** to the respective publications.

Deposition, Visualization and Analysis of Proteomic Data

The mass spectrometry proteomics data have been deposited to the ProteomeXchange Consortium via the PRIDE (Perez-Riverol et al., 2019) partner repository with dataset identifier PXD020007. Pie chart, scatter plots, volcano plot and heatmap were prepared in Microsoft Excel 2013 and GraphPad Prism 8. Area-proportional Venn diagrams were prepared using BioVenn (Hulsen et al., 2008)[2]. Trans-membrane domains were predicted using TMHMM Server v. 2.0 (Krogh et al., 2001)[3] and Phobius (Käll et al., 2007)[4].

RESULTS

Proteome Analysis of CNS Myelin

To purify CNS myelin, we applied an established protocol (Erwig et al., 2019a) to prepare a light-weight membrane fraction from the brains of healthy c57Bl/6N-mice at P75. Aiming to systematically identify myelin-associated proteins we used five complementary approaches as summarized in **Figure 1A**. As the most straightforward way of preparing myelin for proteomic analysis, we separated proteins by 1D-SDS-PAGE and sectioned the lane into 24 equally sized slices (**Figure 1B**), which we subjected to automated tryptic in-gel digest followed by LC-MS-analysis, thereby identifying 788 proteins (**Supplementary Table S1**). When we subjected myelin to an additional washing step of high-pH and high-salt conditions (**Figure 1B**) to deplete soluble and peripheral membrane proteins before 1D-SDS-PAGE-separation and mass spectrometry, we identified 521 proteins (**Supplementary Table S1**). To establish a reference map of myelin proteins including proteoforms, we increased the

resolving power of protein separation by subjecting myelin to 2D-gel electrophoresis with isoelectric focusing (IEF) in the first and horizontal SDS-PAGE in the second dimension (**Figure 1C**). We stained the comprised proteins with colloidal Coomassie (CBB250), picked CBB250-labeled gel-plugs (i.e., protein spots) for automated tryptic in-gel digestion and identified the proteins by peptide mass fingerprint (PMF) and MS/MS-fragment ion mass spectra, both acquired on a MALDI-TOF mass spectrometer. We identified 181 non-redundant proteins from 352 spots (**Supplementary Table S1**). Thereby we expanded our previous myelin protein map (131 non-redundant proteins from 217 spots, Werner et al., 2007), mainly owing to increased resolution in the first dimension by utilizing longer IEF-strips with a wider pH-range (Erwig et al., 2019a). When comparing the proteins identified using the three gel-based approaches we found a total of 930 proteins with a fair overlap (**Figure 1D**).

Considering that contemporary gel-free, label-free proteomic approaches allow the simultaneous identification and quantification of proteins (Neilson et al., 2011; Distler et al., 2014b) we subjected myelin to a workflow of solubilization using ASB-14 and high-urea conditions, automated tryptic in-solution digest by filter-aided sample preparation (FASP), fractionation of peptides by nanoUPLC, and ESI-QTOF mass spectrometry. This workflow was recently established for peripheral myelin (Siems et al., 2020). Importantly, the utilized data-independent acquisition (DIA)-strategy with data acquisition in the MS^E-mode allows the simultaneous quantification and identification of all peptides entering the mass spectrometer, and thereby, when signal intensities are correlated with a spike protein of known concentration (TOP3 method; Silva et al., 2006; Ahrné et al., 2013) the reliable quantification of proteins based on peptide intensities. When subjecting myelin to LC-MS-analysis using MS^E we quantified 393 proteins (**Supplementary Table S1**; labeled in orange in **Figure 1E**) with a false discovery rate (FDR) of <1% and an average sequence coverage of 38.6%. Notably, MS^E quantitatively covered myelin proteins with a dynamic range of over four orders of magnitude parts per million (ppm), thereby allowing quantification of the exceptionally abundant PLP and MBP. When using the ultra-definition (UD)-MS^E-mode, in which the ion mobility option provides an orthogonal dimension of peptide separation after liquid chromatography and before mass measurement, we identified and quantified 809 proteins (**Supplementary Table S1**; labeled in blue in **Figure 1E**) with an average sequence coverage of 35.0%. UDMS^E thus identified about twice as many proteins as MS^E. However, the larger number of proteins identified by UDMS^E went along with a compressed dynamic range of about three orders of magnitude ppm, which is insufficient to reliably quantify the most abundant myelin constituents including PLP, MBP, and CNP. The data acquisition mode-dependent differences in both numbers of quantified proteins and dynamic range are best explained by UDMS^E achieving more efficient precursor-fragment ion alignment and precursor fragmentation upon ion mobility separation of peptides (Distler et al., 2014a, 2016) which causes a ceiling effect for the detection of exceptionally intense peptide signals and thus a compressed dynamic range as previously observed for PNS myelin (Siems et al., 2020).

---

[2]https://www.biovenn.nl/

[3]www.cbs.dtu.dk/services/TMHMM

[4]http://phobius.sbc.su.se/
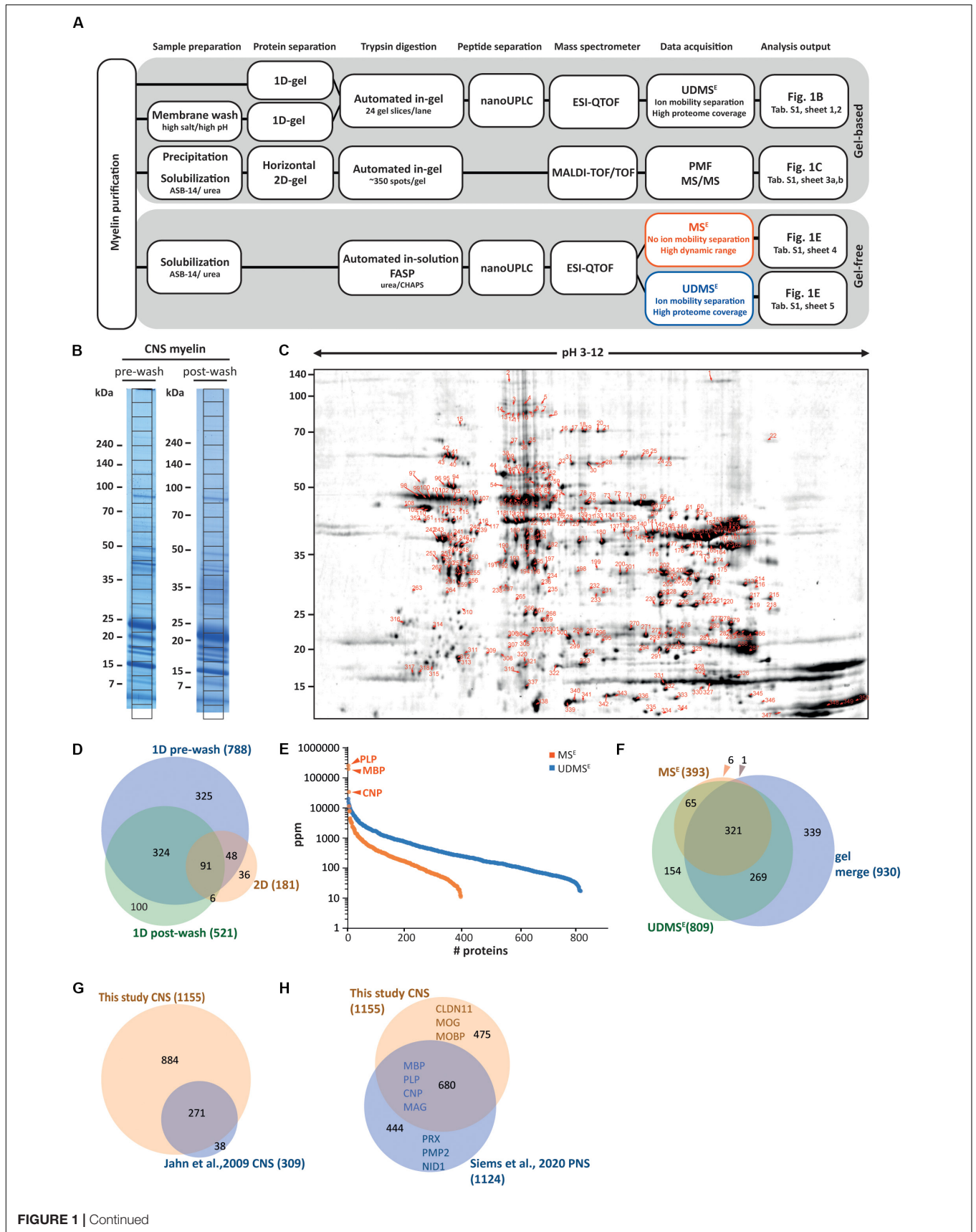
FIGURE 1 | Continued

FIGURE 1 | Proteome analysis of CNS myelin. **(A)** Schematic illustration of the gel-based (top) and gel-free (bottom) proteomic workflow to approach CNS myelin purified from the brains of wild-type c57Bl/6N mice dissected at P75. Note that gel-free proteome analysis enables largely automated sample processing and omits labor-intense gel-electrophoresis, thus reducing hands-on time. **(B)** One-dimensional gel-separation of CNS myelin. Myelin was separated by SDS-PAGE without (pre-wash) or upon (post-wash) depleting soluble and peripheral membrane proteins by an additional step of high-pH and high-salt conditions. Proteins were visualized with colloidal Coomassie (CBB250). The denoted grid subdivides each lane into 24 equally sized slices, which were excised for automated tryptic digest, peptide separation by nanoUPLC and data acquisition using an ESI-QTOF mass spectrometer, thereby identifying 788 (pre-wash) and 521 (post-wash) proteins, respectively (see **Supplementary Table S1**). **(C)** Two-dimensional gel-separation of CNS myelin. Myelin was two-dimensionally separated using a 2D-IEF/SDS-PAGE with isoelectric focusing (IEF) in a 24 cm gel strip with nonlinear pH-gradient (pH 3–12) as the first and 10–15% acrylamide gradient SDS-PAGE (25.5 × 20 cm, gel thickness 0.65 mm) as the second dimension. Proteins were visualized by colloidal Coomassie staining; protein spots were excised, subjected to automated tryptic in-gel digestion and MALDI-TOF mass spectrometry, thereby identifying 181 non-redundant proteins from 352 spots (**Supplementary Table S1**). **(D)** Venn diagram comparing the number of proteins identified in CNS myelin by the three gel-based approaches. **(E)** Number and relative abundance of proteins identified in myelin purified from the brains of wild-type mice using two gel-free data acquisition modes (MS[E], UDMS[E]). Note that MS[E] (orange) identifies comparatively fewer proteins in purified myelin but provides a dynamic range of more than four orders of magnitude. UDMS[E] (blue) identifies a larger number of proteins but provides a dynamic range of only about three orders of magnitude. Note that the dynamic range of MS[E] is required for the quantification of the exceptionally abundant myelin proteins proteolipid protein (PLP), myelin basic protein (MBP) and cyclic nucleotide phosphodiesterase (CNP). Samples were analyzed in three biological replicates with four technical replicates each (duplicate digestion and injection). For datasets see **Supplementary Table S1**. ppm, parts per million. **(F)** Venn diagram comparing the number of proteins identified in CNS myelin by MS[E], UDMS[E] and gel-based approaches. **(G)** Venn diagram of the proteins identified in CNS myelin in this study compared with those identified in a previous approach (Jahn et al., 2009). **(H)** Venn diagram comparing the proteins identified in CNS myelin in this study with those previously identified in PNS myelin (Siems et al., 2020). Selected marker proteins are denoted.

When comparing the proteins identified by MS[E], UDMS[E] and gel-based approaches we found a reasonably high overlap (**Figure 1F**). Comparison of the 1155 proteins identified in CNS myelin in the present study with those 309 identified >10 years ago with the methodological standards of that time (Jahn et al., 2009) shows a remarkably high overlap as well as an about three-fold increase in the number of identified proteins (**Figure 1G**). Notwithstanding that a number of the identified proteins will originate from other cellular sources that contaminate purified myelin, we believe that many of them are indeed low-abundant constituents of the non-compact compartments of myelin.

A comparison of the proteins identified in CNS myelin with the recently established PNS myelin proteome (Siems et al., 2020) confirms that numerous proteins are present in both, but also that many proteins were identified exclusively in either CNS or PNS myelin (**Figure 1H**). Together, the evolving technical standards of in-solution sample preparation and MS[E]-type DIA mass spectrometry allows to comprehensively identify and quantify proteins in myelin. However, only MS[E] (but not UDMS[E]) provides a dynamic range suited to address the relative abundance of the exceptionally abundant PLP, MBP, and CNP. As importantly, the evolution of gel-free methods shifts the major workload in myelin proteome analysis from manual sample handling to data analysis, with much less hands-on time required when compared to gel-based approaches.
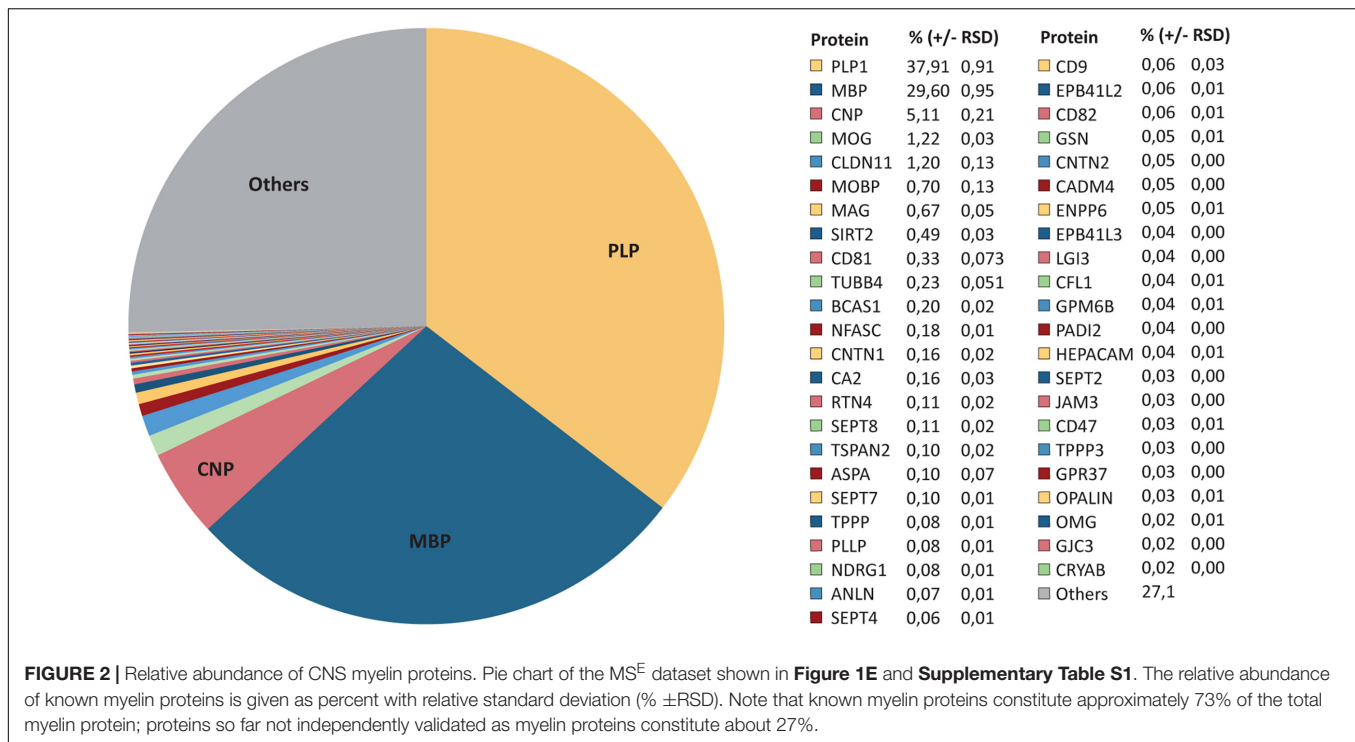
Relative Abundance of CNS Myelin Proteins

As MS[E] provides the best possible dynamic range (**Figure 1E**), we evaluated the relative abundance of all 393 proteins identified in myelin by MS[E] (**Figure 2** and **Supplementary Table S1**). As per this dataset PLP constitutes 38% of the total myelin protein [±1% relative standard deviation (RSD)]. MBP, CNP, and MOG constitute 30% (±1%), 5% (±0.2%), and 1% (±0.03%) of the total myelin protein, respectively (**Figure 2**). However, the present assessment of CNS myelin by MS[E] extends well beyond the most abundant myelin constituents,

thus quantifying known myelin proteins including the tetraspan-proteins CLDN11, CD81, TSPAN2, PLLP, CD9, CD82, GPM6B, and GJC3, the immunoglobulin-domain containing cell-surface proteins MAG, NFASC, CNTN1, RTN4, CNTN2, CADM4, HEPACAM, JAM3, CD47, and OMG, the enzymes SIRT2, CA2, and ASPA, the cytoskeletal and cytoskeleton-associated proteins TUBB4, SEPT2, SEPT4, SEPT7, SEPT8, TPPP, ANLN, GSN, CFL1, and PADI2 as well as MOBP, BCAS1, NDRG1, opalin, and CRYAB (**Figure 2**). By MS[E], 46 known myelin proteins account for approximately 80% of the total myelin protein (**Figure 2**). The remaining 27% is constituted by 347 proteins not yet validated as myelin constituents by independent methods.

Comparison to Related Datasets

An increasing number of studies provides mRNA or protein abundance profiles of myelin or oligodendrocytes. To systematically compare the CNS myelin proteome with these profiles, we correlated our MS[E]-dataset (**Figure 2** and **Supplementary Table S1**) via the gene name entries with related datasets for which quantitative information is publicly available (**Figure 3**).

We first plotted the present MS[E] and UDMS[E]-datasets (**Supplementary Table S1**) against each other (**Figure 3A**). Considering that the same starting material has been assessed it is not unexpected that the datasets correlate well, as reflected by a correlation coefficient of 0.90 (**Figure 3A**). Most visibly diverging from the linear regression line are the most abundant myelin proteins PLP, MBP, CNP, MOG, and CLDN11, reflecting that the dynamic range of UDMS[E] is compressed in the high ppm-range compared to that of MS[E] (also see **Figure 1E**). We then compared the present MS[E]-dataset with an independent myelin proteome dataset previously established by MS[E] (Jahn et al., 2009). We calculated a somewhat lower correlation coefficient of 0.74 (**Figure 3B**), probably owing to the previous use of a predecessor mass spectrometer generation that provided a considerably lower dynamic range. Yet, in conjunction with the high overlap

Protein	%	(+/- RSD)	Protein	%	(+/- RSD)
PLP1	37,91	0,91	CD9	0,06	0,03
MBP	29,60	0,95	EPB41L2	0,06	0,01
CNP	5,11	0,21	CD82	0,06	0,01
MOG	1,22	0,03	GSN	0,05	0,01
CLDN11	1,20	0,13	CNTN2	0,05	0,00
MOBP	0,70	0,13	CADM4	0,05	0,00
MAG	0,67	0,05	ENPP6	0,05	0,01
SIRT2	0,49	0,03	EPB41L3	0,04	0,00
CD81	0,33	0,073	LGI3	0,04	0,00
TUBB4	0,23	0,051	CFL1	0,04	0,01
BCAS1	0,20	0,02	GPM6B	0,04	0,01
NFASC	0,18	0,01	PADI2	0,04	0,00
CNTN1	0,16	0,02	HEPACAM	0,04	0,01
CA2	0,16	0,03	SEPT2	0,03	0,00
RTN4	0,11	0,02	JAM3	0,03	0,00
SEPT8	0,11	0,02	CD47	0,03	0,01
TSPAN2	0,10	0,02	TPPP3	0,03	0,00
ASPA	0,10	0,07	GPR37	0,03	0,00
SEPT7	0,10	0,01	OPALIN	0,03	0,01
TPPP	0,08	0,01	OMG	0,02	0,01
PLLP	0,08	0,01	GJC3	0,02	0,00
NDRG1	0,08	0,01	CRYAB	0,02	0,00
ANLN	0,07	0,01	Others	27,1	
SEPT4	0,06	0,01			

FIGURE 2 | Relative abundance of CNS myelin proteins. Pie chart of the MS[E] dataset shown in **Figure 1E** and **Supplementary Table S1**. The relative abundance of known myelin proteins is given as percent with relative standard deviation (% ±RSD). Note that known myelin proteins constitute approximately 73% of the total myelin protein; proteins so far not independently validated as myelin proteins constitute about 27%.

between the proteins identified in the present and the previous study (Jahn et al., 2009) (**Figure 1G**), myelin proteome analysis emerges as fairly robust across independently purified starting material and different generations of mass spectrometers. We next compared the MS[E]-dataset to the proteome of acutely isolated O4-immunopositive oligodendrocytes (**Figure 3C**) as determined by label-free quantification (LFQ) using data-dependent acquisition (DDA) on an orbitrap mass spectrometer and MaxQuant-software (Sharma et al., 2015). The O4-antibody preferentially immunolabels oligodendrocytes at the progenitor (OPC) and pre-myelinating stages (Sommer and Schachner, 1981; Bansal et al., 1989; Goldman and Kuypers, 2015); the correlation coefficient was calculated as 0.16 (**Figure 3C**). A correlation coefficient of 0.02 (**Figure 3D**) was found when comparing the MS[E]-dataset with the LFQ-intensity profile of O1-immunopositive primary oligodendrocytes after 4 days in vitro (DIV) (Sharma et al., 2015). The myelin proteome as determined here is thus more closely related to the proteome of acutely isolated O4-immunopositive oligodendrocytes than to that of O1-immunopositive primary oligodendrocytes 4 DIV.

We then compared the MS[E]-dataset with various available mRNA-abundance profiles. When comparing the MS[E]-dataset to the transcriptome of purified CNS myelin as determined by RNA-seq (Thakurela et al., 2016) we calculated a correlation coefficient of 0.27 (**Figure 3E**). Interestingly, the comparison between the MS[E]-dataset and the RNA-seq-based transcriptome of oligodendrocytes immunopanned from the cortex using antibodies against MOG (Zhang et al., 2014) revealed a roughly comparable correlation coefficient of 0.31 (**Figure 3F**). Notably, MOG-immunopositivity labels myelinating oligodendrocytes,

implying that the stage of oligodendrocyte differentiation must be considered when judging dataset correlations. It is thus not surprising that a somewhat lower correlation coefficient of 0.10 (**Figure 3G**) was calculated when comparing the MS[E]-dataset with the RNA-seq-based transcriptome of acutely isolated O4[+]-oligodendrocytes (Sharma et al., 2015). Finally, we compared the MS[E]-dataset to several scRNA-seq-based transcriptome datasets (Zeisel et al., 2015; Marques et al., 2016; Falcão et al., 2018). To this aim we calculated the mean transcript abundance as average count reads per unique molecular identifier (UMI) of the cells in those clusters that reflect mature oligodendrocytes. When comparing the MS[E]-dataset to mature oligodendrocytes sorted from the mouse cortex and hippocampus [all 484 cells in clusters Oligo5 and Oligo6 in Zeisel et al. (2015)], we find a correlation coefficient of 0.24 (**Figure 3H**). Importantly, we find a roughly similar correlation coefficient when comparing the MS[E]-dataset to mature oligodendrocytes sorted from 10 regions of the mouse CNS [all 2748 cells in clusters MOL1–MOL6 in Marques et al. (2016)] (**Figure 3I**) or to mature oligodendrocytes sorted from the spinal cord of mice [all 617 cells in clusters MOL2-Ct and MOL5/6-Ct in Falcão et al. (2018)] (**Figure 3J**).

Together, when judging correlations between large datasets evaluating mRNA and protein abundance profiles of oligodendrocytes and myelin, aspects to be considered include the method of sample preparation, the stage of oligodendrocyte differentiation and the methodology of analysis. Yet, roughly similar correlation coefficients were calculated when comparing the myelin proteome with various proteomic and transcriptomic approaches to the molecular profiles of oligodendrocytes.
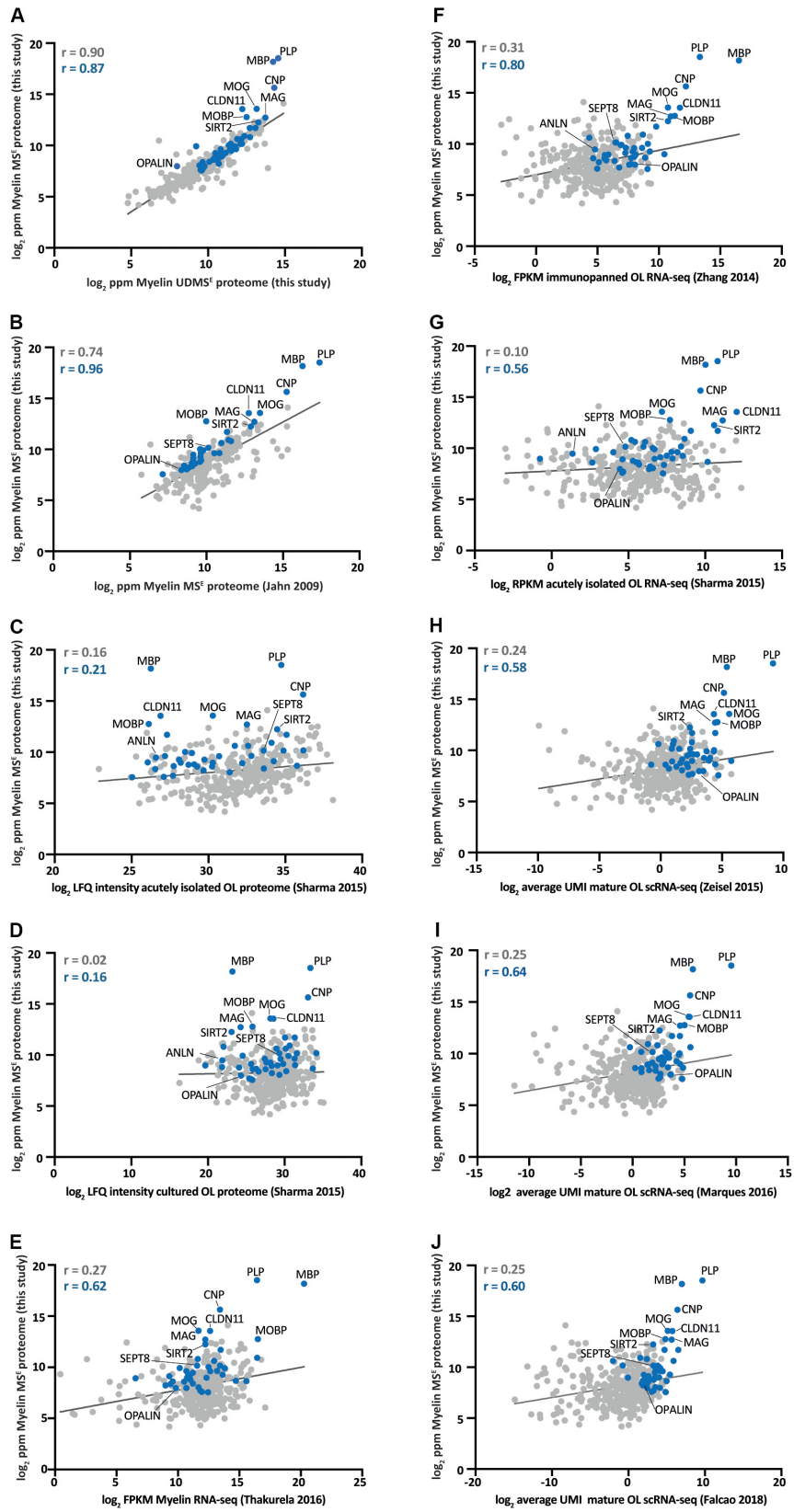
FIGURE 3 | Continued

FIGURE 3 | Comparison of the myelin proteome with proteome and transcriptome profiles of myelin and oligodendrocytes. **(A)** Log$_2$-transformed relative abundance of the proteins identified in myelin in this study by MS^E plotted against their log$_2$-transformed relative abundance as quantified by UDMS^E. Data points representing known myelin proteins as specified in **Figure 2** are labeled in blue; all other data points in gray. The correlation coefficient (*r*) was calculated for all proteins identified by MS^E (displayed in gray) and specifically for the known myelin proteins (given in blue). The regression line is plotted for orientation. ppm, parts per million. **(B)** Same as **(A)** but plotted against the myelin proteome as previously assessed by MS^E (Jahn et al., 2009). **(C)** Same as **(A)** but plotted against the proteome of acutely isolated O4-immunopositive oligodendrocytes (Sharma et al., 2015). LFQ, label-free quantification. **(D)** Same as **(A)** but plotted against the proteome of O1-immunopositive primary oligodendrocytes cultured for 4 days *in vitro* (DIV) (Sharma et al., 2015). **(E)** Same as **(A)** but plotted against the RNA-seq-based transcriptome of myelin purified from the brains of mice (Thakurela et al., 2016). FPKM, fragments per kilobase of exon model per million reads mapped. **(F)** Same as **(A)** but plotted against the RNA-seq-based transcriptome of oligodendrocytes immunopanned using MOG-specific antibodies (Zhang et al., 2014). **(G)** Same as **(A)** but plotted against the RNA-seq-based transcriptome of acutely isolated O4-immunopositive oligodendrocytes (Sharma et al., 2015). RPKM, reads per kilobase per million mapped reads. **(H)** Same as **(A)** but plotted against the scRNA-seq-based transcriptome of mature oligodendrocytes in the mouse cortex and hippocampus [mean of all 484 cells in clusters Oligo5 and Oligo6 in Zeisel et al. (2015)]. UMI, unique molecular identifiers. **(I)** Same as **(A)** but plotted against the scRNA-seq-based transcriptome of mature oligodendrocytes in 10 regions of the mouse CNS [mean of all 2748 cells in clusters OL1 – OL6 in Marques et al. (2016)]. **(J)** Same as **(A)** but plotted against the scRNA-seq-based transcriptome of mature oligodendrocytes in the mouse spinal cord [mean of all 617 cells in clusters MOL2-Ct and MOL5/6-Ct in Falcão et al. (2018)].

Persistence of the Myelin Proteome Upon Post-mortem Delay

Autopsy material from human patients and healthy-appearing controls is increasingly evaluated by systematic molecular profiling, as exemplified by the recent snRNA-seq-based assessment of oligodendroglial transcriptional profiles in multiple sclerosis patients (Jäkel et al., 2019). Notably, the use of autopsy material involves a post-mortem delay between the death of a subject and the collection of a biopsy. However, post-mortem delay may affect sample integrity and thus data validity. Considering that proteomic analysis of myelin in mice is usually performed upon freezing of samples immediately after dissection, we asked whether the myelin proteome can also be assessed upon post-mortem delay. We thus purified myelin from the brains of c57Bl/6N-mice to compare the myelin proteome between mice after a post-mortem delay of 6 h at room temperature with that of mice upon sample freezing immediately after dissection. Upon SDS-PAGE-separation and silver staining, no signs of major degradation were evident and the band patterns appeared essentially similar (**Figure 4A**). We next subjected myelin to routine differential proteome profiling by UDMS^E with dynamic range enhancement (DRE-UDMS^E) (**Supplementary Table S2**). Using this data acquisition mode with intermediate features as to identification rates and dynamic range (for methodological details see Siems et al., 2020) we found that known myelin proteins displayed only minor differences as visualized in a volcano plot (red data points in **Figure 4B**) and a heatmap (**Figure 4C**). Indeed, no known myelin protein exceeded the threshold of a log$_2$-fold transformed fold-change (FC) of $-1/+1$, i.e., a 2-fold increased or 0.5-fold diminished relative abundance. Together, the myelin proteome displays only minor changes upon a post-mortem delay of 6 h, implying that proteomic assessment of myelin purified from autopsy samples appears feasible.

DISCUSSION

Understanding the molecular complexity of the nervous system involves molecular profiling of cells and cellular specializations including myelin. Here we combined various proteomic approaches for comprehensive coverage of the CNS myelin proteome and identified 1155 proteins in myelin biochemically purified from the brains of mice. We note that gel-based methods involving separation at the protein level facilitated a slightly higher identification rate compared to gel-free methods comprising *in situ*-digestion of the entire proteome, likely because of the pre-fractionation effect inherent to the former. On the other hand, gel-free data acquisition by UDMS^E also enabled deep qualitative coverage while necessitating considerably less input material and manual sample handling.

Importantly, the MS^E-data acquisition mode covered a dynamic range of over four orders of magnitude of protein abundance. Indeed, compared to a previous approach (Jahn et al., 2009) the technical advancements implemented in the current mass spectrometer generation now allow reliable quantification of myelin proteins spanning from the exceptionally abundant PLP and MBP to low-abundant constituents including oligodendrocyte myelin glycoprotein (OMG) (Wang et al., 2002), oligodendrocytic myelin paranodal and inner loop protein (OPALIN) (Golan et al., 2008; Kippert et al., 2008) and the G-protein coupled receptor GPR37 (Yang et al., 2016). For PLP, MBP and CNP our quantification is in accordance with but specifies prior estimates based on 1D-gel separation and various protein staining techniques, in which they were proposed to constitute 30–45%, 22–35%, and 4–15% of the total myelin protein, respectively (Morell et al., 1972, 1973; Banik and Smith, 1977; Deber and Reynolds, 1991). Notably, it also shifts our previous MS^E-based estimates for PLP and MBP (Jahn et al., 2009) toward higher relative abundance, with the lower dynamic range of the mass spectrometers at that time being the most likely reason for the former under-quantification. It is not surprising that PLP, MBP, and CNP have overshadowed less abundant myelin constituents in initial gel-based approaches when considering the exceptional dynamic range of the relative abundance of myelin proteins. Together, the myelin proteome provided here provides an updated comprehensive compendium and re-adjusts the relative abundance of CNS myelin proteins.

Do true myelin proteins exist that escape proteomic identification? As exemplified by myelin and lymphocyte protein (MAL) (Schaeren-Wiemers et al., 2004), the tryptic digest of
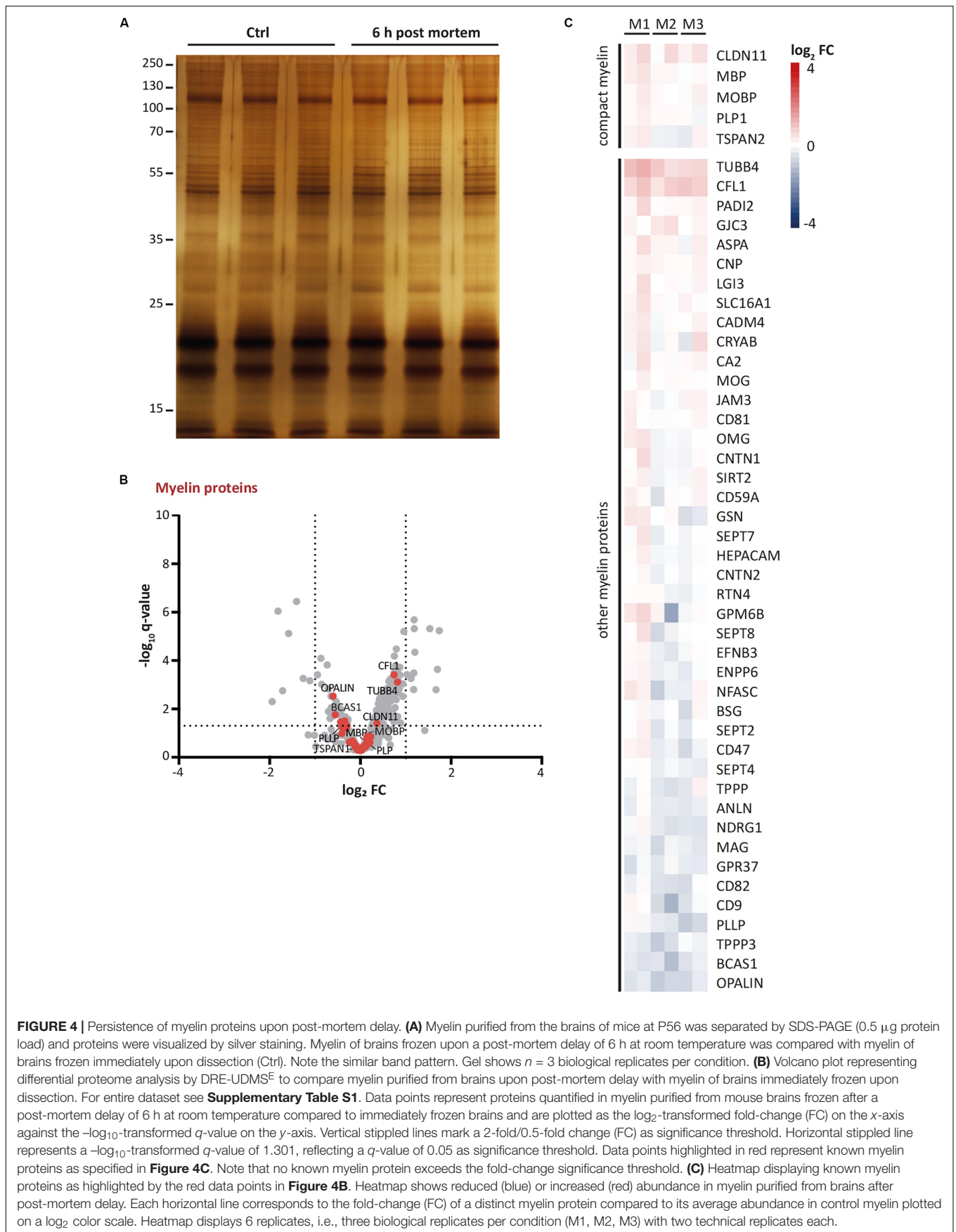
FIGURE 4 | Persistence of myelin proteins upon post-mortem delay. **(A)** Myelin purified from the brains of mice at P56 was separated by SDS-PAGE (0.5 μg protein load) and proteins were visualized by silver staining. Myelin of brains frozen upon a post-mortem delay of 6 h at room temperature was compared with myelin of brains frozen immediately upon dissection (Ctrl). Note the similar band pattern. Gel shows $n = 3$ biological replicates per condition. **(B)** Volcano plot representing differential proteome analysis by DRE-UDMS^E to compare myelin purified from brains upon post-mortem delay with myelin of brains immediately frozen upon dissection. For entire dataset see **Supplementary Table S1**. Data points represent proteins quantified in myelin purified from mouse brains frozen after a post-mortem delay of 6 h at room temperature compared to immediately frozen brains and are plotted as the $\log_2$-transformed fold-change (FC) on the x-axis against the $-\log_{10}$-transformed q-value on the y-axis. Vertical stippled lines mark a 2-fold/0.5-fold change (FC) as significance threshold. Horizontal stippled line represents a $-\log_{10}$-transformed q-value of 1.301, reflecting a q-value of 0.05 as significance threshold. Data points highlighted in red represent known myelin proteins as specified in **Figure 4C**. Note that no known myelin protein exceeds the fold-change significance threshold. **(C)** Heatmap displaying known myelin proteins as highlighted by the red data points in **Figure 4B**. Heatmap shows reduced (blue) or increased (red) abundance in myelin purified from brains after post-mortem delay. Each horizontal line corresponds to the fold-change (FC) of a distinct myelin protein compared to its average abundance in control myelin plotted on a $\log_2$ color scale. Heatmap displays 6 replicates, i.e., three biological replicates per condition (M1, M2, M3) with two technical replicates each.

TABLE 1 | Comparison of proteins identified in CNS myelin and disease genes associated with white matter pathology.

Protein name	Gene symbol	OMIM#	Gene Locus	Disease
Aldehyde dehydrogenase 3a2	ALDH3A2	609523	17p11.2	Sjogren-Larsson Syndrome
Aspartoacylase	ASPA	608034	17p13.2	Canavan disease
Atlastin GTPase 1	ATL1	606439	14q22.1	SPG 3A
Cathepsin D	CTSD	610127	11p15.5	Ceroid lipofuscinosis
Contactin-associated protein 1	CNTNAP1	602346	17q21.2	LCCS 7
Cyclic nucleotide phosphodiesterase	CNP	123830	17q21.2	HLD
Dynamin 2	DNM2	602378	19p13.2	LCCS 5
Endoplasmic reticulum lipid raft-associated protein 2	ERLIN2	611605	8p11.23	SPG 18
Glial fibrillary acidic protein	GFAP	137780	17q21.31	Alexander disease
Glutamate-Ammonia ligase	GLUL	138290	1q25.3	Glutamine-deficiency, congenital
Heat-shock 60-kD protein 1	HSPD1	118190	2q33.1	HLD 4, SPG 13
Hepatocyte cell adhesion molecule	HEPACAM	611642	11q24.2	MLC 2
Junctional adhesion molecule 3	JAM3	613730	11q25	HDBSCC
Magnesium transporter NIPA1	NIPA1	608145	15q11.2	SPG 6
Monoacylglycerol lipase ABHD12	ABHD12	613599	20p11.21	PHARC
Myelin basic protein	MBP	159430	18q23	18q deletion syndrome
Myelin-associated glycoprotein	MAG	159460	19q13.12	SPG 75
Myelin-oligodendrocyte glycoprotein	MOG	159465	6p22.1	Narcolepsy 7
Neurofascin	NFASC	609145	1q32.1	NEDCPMD
Phosphoglycerate dehydrogenase	PHGDH	606879	1p12	PHGDH deficiency, NLS 1
Phosphoserine aminotransferase 1	PSAT1	610936	9q21.2	PSAT deficiency, NLS 2
Prosaposin	PSAP	176801	10q22.1	Metachromatic Leukodystrophy
Proteolipid protein	PLP1	300401	Xq22.2	Pelizaeus-Merzbacher disease, SPG 2
Transmembrane protein 63a	TMEM63A	618685	1q42.12	HLD 19
Tubulin beta 4a	TUBB4A	602662	19p13.3	Dystonia 4, HLD 6

Proteins listed fulfill three criteria: (1) mass spectrometric identification in purified CNS myelin, (2) transcript expression in oligodendrocytes and (3) gene mutations associated with diseases involving pathology of myelin or the white matter. For some of the proteins with additional expression in astrocytes, microglia or neurons it is presently unknown whether loss/gain of function in oligodendrocytes is causative of the disease. HLD, Hypomyelinating Leukodystrophy; SPG, Spastic Paraplegia; LCCS, Lethal Congenital Contracture Syndrome; MLC, Megalencephalic leukoencephalopathy with subcortical cysts; NLS, Neu-Laxova syndrome; HDBSCC, Hemorrhagic destruction of the brain, subependymal calcification and cataracts; PHARC, polyneuropathy, hearing loss, ataxia, retinitis pigmentosa and cataract; NEDCPMD, neurodevelopmental disorder with central and peripheral motor dysfunction.

some myelin proteins may result in peptides incompatible with mass spectrometric detection; their identification would require the use of proteases other than trypsin. We also note that some low-abundant signaling proteins with potent functions in regulating myelination may be assumed to localize to myelin *in vivo* but were not mass spectrometrically identified, as exemplified by the G-protein coupled receptors GPR17 (Chen et al., 2009) and GPR56/ADGRG1 (Ackerman et al., 2015; Giera et al., 2015) and the Ig-domain containing LINGO1 (Mi et al., 2005). It is currently speculative if these proteins are preferentially expressed in oligodendroglial cell bodies rather than myelin membranes or during the stages of oligodendrocyte differentiation that precede myelination. It is also speculative if enhanced mass spectrometric sensitivity would facilitate their identification in myelin. Indeed, we can not formally exclude that these proteins may be identified if less rigorous criteria were applied (e.g., demanding only one peptide per protein), which may be sufficient for identification but not for the reliable quantification of proteins as aimed at in the present study. Importantly, however, lower stringency may not only identify more true myelin constituents but also false-positive hits. This is a concern, in particular when considering that the myelin-enriched fraction may comprise up to 5% contaminants

from other cellular sources (De Monasterio-Schrader et al., 2012). We note that currently no biochemical method is available that allows preventing this limitation. Yet, comparing various datasets yields systematic information, for example on the presence of a transcript in oligodendrocytes as expected for a CNS myelin protein.

Mutations affecting genes that encode classical myelin proteins including PLP, CNP, MAG, TUBB4, and ASPA cause severe neurological disorders including hypomyelinating leukodystrophies (HLD) and spastic paraplegias (SPG) (Kaul et al., 1993; Saugier-Veber et al., 1994; Simons et al., 2013; Lossos et al., 2015; Al-Abdi et al., 2020) (**Table 1**). However, current sequencing efforts also identify disease-causing genes that encode less well-characterized proteins. Notably, most types of leukodystrophies and spastic paraplegias are caused by mutations affecting genes of which the transcripts are enriched in neurons, astrocytes or microglia rather than oligodendrocytes (Nave and Werner, 2014; van der Knaap et al., 2019). For newly identified disease genes, thus, evaluating mRNA-expression using transcriptome datasets and presence of the protein in myelin using the present myelin proteome resource may serve as a useful entry point into identifying the primarily affected cell type. For example, mutations of the *HSPD1* gene cause

HLD4 or SPG13 (Hansen et al., 2002; Magen et al., 2008) and mutations of the *TMEM63A* gene cause HLD19 (Yan et al., 2019) (**Table 1**). Considering that both transcripts are expressed in oligodendrocytes as per transcriptome datasets and both proteins are comprised in the myelin proteome, the disease mechanisms may involve primary impairment of the biogenesis, maintenance or functions of myelin.

Dysfunctions of oligodendrocytes and myelin contribute to the neuropathology in a growing number of neurodegenerative disorders and their respective mouse models, including Rett syndrome (Nguyen et al., 2013), amyotrophic lateral sclerosis (Kang et al., 2013), Down syndrome (Olmos-Serrano et al., 2016), Alzheimer's disease (Nasrabady et al., 2018) and multiple sclerosis (Factor et al., 2020). Considering that molecular assessments now frequently involve autopsy material, it is motivating that our data imply that myelin proteome analysis appears well possible post-mortem, at least up to a 6 h delay. A systematic understanding of the abundance profiles of all myelin proteins in the healthy brain and in myelin-related disorders may contribute to comprehending myelin-related physiology and pathophysiology. Myelin proteome analysis as pursued here provides a basis for addressing possible proteomic heterogeneity of myelin in dependence of CNS region, age and species, as well as in mouse models and human patients with white matter disorders.

DATA AVAILABILITY STATEMENT

The mass spectrometry proteomics data have been deposited to the ProteomeXchange Consortium via the PRIDE (Perez-Riverol et al., 2019) partner repository with dataset identifier, PXD020007.

ETHICS STATEMENT

Ethical review and approval was not required for the animal study because for the procedure of sacrificing mice for subsequent preparation of tissue, all regulations given in the German animal protection law (TierSchG §4) are followed. Since sacrificing of rodents is not an experiment on animals according to §7 Abs. 2 Satz 3 TierSchG, no specific authorization or notification is required for the present work.

REFERENCES

Ackerman, S. D., Garcia, C., Piao, X., Gutmann, D. H., and Monk, K. R. (2015). The adhesion GPCR Gpr56 regulates oligodendrocyte development via interactions with Gα12/13 and RhoA. *Nat. Commun.* 6:6122. doi: 10.1038/ncomms7122

Ahrné, E., Molzahn, L., Glatter, T., and Schmidt, A. (2013). Critical assessment of proteome-wide label-free absolute abundance estimation strategies. *Proteomics* 13, 2567–2578. doi: 10.1002/pmic.201300135

AUTHOR CONTRIBUTIONS

KK, DH, RJ, TL, and MU performed the experiments. SS analyzed the data and performed the statistical analysis. TS wrote the code to interpret single cell resolution transcriptome data. OJ and HW conceived, designed, and directed the study. HW wrote the manuscript with major contributions by SS and OJ. All the authors contributed to revising the manuscript and approved the submitted version.

FUNDING

ACKNOWLEDGMENTS

SUPPLEMENTARY MATERIAL

The Supplementary Material for this article can be found online at: https://www.frontiersin.org/articles/10.3389/fncel.2020.00239/full#supplementary-material

TABLE S1 | Compendium of the mouse CNS myelin proteome. **(Sheet 1)** 1D gel separation of proteins followed by in-gel digestion and LC-MS analysis (788 proteins). **(Sheet 2)** 1D gel separation of proteins after membrane wash followed by in-gel digestion and LC-MS analysis (521 proteins). **(Sheet 3a)** 2D gel separation of proteins by in-gel digestion and MALDI-TOF-MS: spot annotation of the master gel shown in **Figure 3C** (352 gel spots). **(Sheet 3b)** 2D gel separation of proteins followed by in-gel digestion and MALDI-TOF-MS: non-redundant protein list (181 proteins). **(Sheet 4)** In-solution digestion of proteins and label-free quantification by MS^E (393 proteins). **(Sheet 5)** In-solution digestion of proteins and label-free quantification by UDMS^E (809 proteins). **(Sheet 6)** Compendium providing information on the approach by which a myelin-associated protein was identified and on predicted transmembrane domains (1155 proteins).

TABLE S2 | Label-free quantification of proteins in CNS myelin purified from mouse brains without (Ctrl) and after 6 h post-mortem delay (PMD6h) by DRE-UDMS^E. Related to **Figure 4**. **(Sheet 1)** Dataset.

Al-Abdi, L., Al Murshedi, F., Elmanzalawy, A., Al Habsi, A., Helaby, R., Ganesh, A., et al. (2020). CNP deficiency causes severe hypomyelinating leukodystrophy in humans. *Hum. Genet.* 139, 615–622. doi: 10.1007/s00439-020-02144-4

Ambrozkiewicz, M. C., Schwark, M., Kishimoto-Suga, M., Borisova, E., Hori, K., Salazar-Lázaro, A., et al. (2018). Polarity Acquisition in Cortical Neurons Is Driven by Synergistic Action of Sox9-Regulated Wwp1 and Wwp2 E3 Ubiquitin Ligases and Intronic miR-140. *Neuron* 100:1097-1115.e15. doi: 10.1016/j.neuron.2018.10.008

Banik, N. L., and Smith, M. E. (1977). Protein determinants of myelination in different regions of developing rat central nervous system. *Biochem. J.* 162, 247–255. doi: 10.1042/bj1620247

Bansal, R., Warrington, A. E., Gard, A. L., Ranscht, B., and Pfeiffer, S. E. (1989). Multiple and novel specificities of monoclonal antibodies O1, O4, and R-mAb used in the analysis of oligodendrocyte development. *J. Neurosci. Res.* 24, 548–557. doi: 10.1002/jnr.490240413

Butler, A., Hoffman, P., Smibert, P., Papalexi, E., and Satija, R. (2018). Integrating single-cell transcriptomic data across different conditions, technologies, and species. *Nat. Biotechnol.* 36, 411–420. doi: 10.1038/nbt.4096

Chen, Y., Wu, H., Wang, S., Koito, H., Li, J., Ye, F., et al. (2009). The oligodendrocyte-specific G protein-coupled receptor GPR17 is a cell-intrinsic timer of myelination. *Nat. Neurosci.* 12, 1398–1406. doi: 10.1038/nn.2410

Chrast, R., Saher, G., Nave, K. A., and Verheijen, M. H. G. (2011). Lipid metabolism in myelinating glial cells: Lessons from human inherited disorders and mouse models. *J. Lipid Res.* 52, 419–434. doi: 10.1194/jlr.R009761

De Monasterio-Schrader, P., Jahn, O., Tenzer, S., Wichert, S. P., Patzig, J., and Werner, H. B. (2012). Systematic approaches to central nervous system myelin. *Cell. Mol. Life Sci.* 69, 2879–2894. doi: 10.1007/s00018-012-0958-9

de Monasterio-Schrader, P., Patzig, J., Möbius, W., Barrette, B., Wagner, T. L., Kusch, K., et al. (2013). Uncoupling of neuroinflammation from axonal degeneration in mice lacking the myelin protein tetraspanin-2. *Glia* 61, 1832–1847. doi: 10.1002/glia.22561

Deber, C. M., and Reynolds, S. J. (1991). Central nervous system myelin: structure, function, and pathology. *Clin. Biochem.* 24, 113–134. doi: 10.1016/0009-9120(91)90421-A

Denninger, A. R., Breglio, A., Maheras, K. J., Leduc, G., Cristiglio, V., Demé, B., et al. (2015). Claudin-11 tight junctions in myelin are a barrier to diffusion and lack strong adhesive properties. *Biophys. J.* 109, 1387–1397. doi: 10.1016/j.bpj.2015.08.012

Dhaunchak, A. S., Huang, J. K., De Faria, O., Roth, A. D., Pedraza, L., Antel, J. P., et al. (2010). A proteome map of axoglial specializations isolated and purified from human central nervous system. *Glia* 58, 1949–1960. doi: 10.1002/glia.21064

Distler, U., Kuharev, J., Navarro, P., Levin, Y., Schild, H., and Tenzer, S. (2014a). Drift time-specific collision energies enable deep-coverage data-independent acquisition proteomics. *Nat. Methods* 11, 167–170. doi: 10.1038/nmeth.2767

Distler, U., Kuharev, J., and Tenzer, S. (2014b). Biomedical applications of ion mobility-enhanced data-independent acquisition-based label-free quantitative proteomics. *Expert Rev. Proteomics* 11, 675–684. doi: 10.1586/14789450.2014.971114

Distler, U., Kuharev, J., Navarro, P., and Tenzer, S. (2016). Label-free quantification in ion mobility–enhanced data-independent acquisition proteomics. *Nat. Protoc.* 11, 795–812. doi: 10.1038/nprot.2016.042

Edgar, J. M., McLaughlin, M., Werner, H. B., McCulloch, M. C., Barrie, J. A., Brown, A., et al. (2009). Early ultrastructural defects of axons and axon-glia junctions in mice lacking expression of Cnp1. *Glia* 57, 1815–1824. doi: 10.1002/glia.20893

Erwig, M. S., Hesse, D., Jung, R. B., Uecker, M., Kusch, K., Tenzer, S., et al. (2019a). 'Myelin: Methods for Purification and Proteome Analysis'. *Methods Mol. Biol.* 1936, 37–63. doi: 10.1007/978-1-4939-9072-6_3

Erwig, M. S., Patzig, J., Steyer, A. M., Dibaj, P., Heilmann, M., Heilmann, I., et al. (2019b). Anillin facilitates septin assembly to prevent pathological outfoldings of central nervous system myelin. *eLife* 8:e43888. doi: 10.7554/eLife.43888

Factor, D. C., Barbeau, A. M., Allan, K. C., Hu, L. R., Madhavan, M., Hoang, A. T., et al. (2020). Cell type-specific intralocus interactions reveal oligodendrocyte mechanisms in MS. *Cell* 181:382-395.e21. doi: 10.1016/j.cell.2020.03.002

Falcão, A. M., van Bruggen, D., Marques, S., Meijer, M., Jäkel, S., Agirre, E., et al. (2018). Disease-specific oligodendrocyte lineage cells arise in multiple sclerosis. *Nat. Med.* 24, 1837–1844. doi: 10.1038/s41591-018-0236-y

Giera, S., Deng, Y., Luo, R., Ackerman, S. D., Mogha, A., Monk, K. R., et al. (2015). The adhesion G protein-coupled receptor GPR56 is a cell-autonomous regulator of oligodendrocyte development. *Nat. Commun.* 6:6121. doi: 10.1038/ncomms7121

Golan, N., Adamsky, K., Kartvelishvily, E., Brockschnieder, D., Möbius, W., Spiegel, I., et al. (2008). Identification of Tmem10/Opalin as an oligodendrocyte enriched gene using expression profiling combined with genetic cell ablation. *Glia* 56, 1176–1186. doi: 10.1002/glia.20688

Goldman, S. A., and Kuypers, N. J. (2015). How to make an oligodendrocyte. *Development* 142, 3983–3995. doi: 10.1242/dev.126409

Gopalakrishnan, G., Awasthi, A., Belkaid, W., De Faria, O., Liazoghli, D., Colman, D. R., et al. (2013). Lipidome and proteome map of myelin membranes. *J. Neurosci. Res.* 91, 321–334. doi: 10.1002/jnr.23157

Gow, A., Southwood, C. M., Li, J. S., Pariali, M., Riordan, G. P., Brodie, S. E., et al. (1999). CNS Myelin and sertoli cell tight junction strands are absent in OSP/claudin-11 null mice. *Cell* 99, 649–659. doi: 10.1016/S0092-8674(00)81553-6

Hansen, J. J., Dürr, A., Cournu-Rebeix, I., Georgopoulos, C., Ang, D., Nielsen, M. N., et al. (2002). Hereditary spastic paraplegia SPG13 is associated with a mutation in the gene encoding the mitochondrial chaperonin Hsp60. *Am. J. Hum. Genet.* 70, 1328–1332. doi: 10.1086/339935

Hulsen, T., de Vlieg, J., and Alkema, W. (2008). BioVenn – a web application for the comparison and visualization of biological lists using area-proportional Venn diagrams. *BMC Genomics* 9:488. doi: 10.1186/1471-2164-9-488

Ishii, A., Dutta, R., Wark, G. M., Hwang, S. II, Han, D. K., Trapp, B. D., et al. (2009). Human myelin proteome and comparative analysis with mouse myelin. *Proc. Natl. Acad. Sci. U.S.A.* 106, 14605–14610. doi: 10.1073/pnas.0905936106

Jahn, O., Hesse, D., Reinelt, M., and Kratzin, H. D. (2006). Technical innovations for the automated identification of gel-separated proteins by MALDI-TOF mass spectrometry. *Anal. Bioanal. Chem.* 386, 92–103. doi: 10.1007/s00216-006-0592-1

Jahn, O., Tenzer, S., Bartsch, N., Patzig, J., and Werner, H. B. (2013). "Myelin proteome analysis: methods and implications for the myelin cytoskeleton," in *The Cytoskeleton. Neuromethods*, Vol. 79, ed. R. Dermietzel, (Totowa, NJ: Humana Press), doi: 10.1007/978-1-62703-266-7_15

Jahn, O., Tenzer, S., and Werner, H. B. (2009). Myelin proteomics: Molecular anatomy of an insulating sheath. *Mol. Neurobiol.* 40, 55–72. doi: 10.1007/s12035-009-8071-2

Jäkel, S., Agirre, E., Mendanha Falcão, A., van Bruggen, D., Lee, K. W., Knuesel, I., et al. (2019). Altered human oligodendrocyte heterogeneity in multiple sclerosis. *Nature* 566, 543–547. doi: 10.1038/s41586-019-0903-2

Johns, T. G., and Bernard, C. C. A. (1999). The structure and function of myelin oligodendrocyte glycoprotein. *J. Neurochem.* 72, 1–9. doi: 10.1046/j.1471-4159.1999.0720001.x

Joseph, S., Werner, H., and Stegmüller, J. (2019). Gallyas silver impregnation of myelinated nerve fibers. *Bio-Protocol* 9:e3436. doi: 10.21769/bioprotoc.3436

Käll, L., Krogh, A., and Sonnhammer, E. L. L. (2007). Advantages of combined transmembrane topology and signal peptide prediction-the Phobius web server. *Nucleic Acids Res.* 35, W429–W432. doi: 10.1093/nar/gkm256

Kang, S. H., Li, Y., Fukaya, M., Lorenzini, I., Cleveland, D. W., Ostrow, L. W., et al. (2013). Degeneration and impaired regeneration of gray matter oligodendrocytes in amyotrophic lateral sclerosis. *Nat. Neurosci.* 16, 571–579. doi: 10.1038/nn.3357

Kaul, R., Gao, G. P., Balamurugan, K., and Matalon, R. (1993). Cloning of the human aspartoacylase cDNA and a common missense mutation in Canavan disease. *Nat. Genet.* 5, 118–123. doi: 10.1038/ng1093-118

Kippert, A., Trajkovic, K., Fitzner, D., Opitz, L., and Simons, M. (2008). Identification of tmem10/opalin as a novel marker for oligodendrocytes using gene expression profiling. *BMC Neurosci.* 9:40. doi: 10.1186/1471-2202-9-40

Krogh, A., Larsson, B., Von Heijne, G., and Sonnhammer, E. L. L. (2001). Predicting transmembrane protein topology with a hidden Markov model: Application to complete genomes. *J. Mol. Biol.* 305, 567–580. doi: 10.1006/jmbi.2000.4315

Kuharev, J., Navarro, P., Distler, U., Jahn, O., and Tenzer, S. (2015). In-depth evaluation of software tools for data-independent acquisition based label-free quantification. *Proteomics* 15, 3140–3151. doi: 10.1002/pmic.201400396

Lappe-Siefke, C., Goebbels, S., Gravel, M., Nicksch, E., Lee, J., Braun, P. E., et al. (2003). Disruption of Cnp1 uncouples oligodendroglial functions in axonal support and myelination. *Nat. Genet.* 33, 366–374. doi: 10.1038/ng1095

Lee, A. G. (2001). Myelin: delivery by raft. *Curr. Biol.* 11, R60–R62. doi: 10.1016/S0960-9822(01)00008-2

Lossos, A., Ponger, P., Newman, J. P., Elazar, N., Mor, N., Eshed-Eisenbach, Y., et al. (2015). Myelin-associated glycoprotein gene mutation causes Pelizaeus-Merzbacher disease-like disorder. *Brain* 138, 2521–2536. doi: 10.1093/brain/awv204

Magen, D., Georgopoulos, C., Bross, P., Ang, D., Segev, Y., Goldsher, D., et al. (2008). Mitochondrial Hsp60 chaperonopathy causes an autosomal-recessive neurodegenerative disorder linked to brain hypomyelination and leukodystrophy. *Am. J. Hum. Genet.* 83, 30–42. doi: 10.1016/j.ajhg.2008.05.016

Magno-Sumbilla, C., and Campagnoni, A. T. (1977). Factors affecting the electrophoretic analysis of myelin proteins: Application to changes occurring during brain development. *Brain Res.* 126, 131–148. doi: 10.1016/0006-8993(77)90220-7

Manrique-Hoyos, N., Jürgens, T., Grønborg, M., Kreutzfeldt, M., Schedensack, M., Kuhlmann, T., et al. (2012). Late motor decline after accomplished remyelination: Impact for progressive multiple sclerosis. *Ann. Neurol.* 71, 227–244. doi: 10.1002/ana.22681

Marques, S., Zeisel, A., Codeluppi, S., van Bruggen, D., Mendanha Falcao, A., Xiao, L., et al. (2016). Oligodendrocyte heterogeneity in the mouse juvenile and adult central nervous system. *Science* 352, 1326–1329. doi: 10.1126/science.aaf6463

Mi, S., Miller, R. H., Lee, X., Scott, M. L., Shulag-Morskaya, S., Shao, Z., et al. (2005). LINGO-1 negatively regulates myelination by oligodendrocytes. *Nat. Neurosci.* 8, 745–751. doi: 10.1038/nn1460

Möbius, W., Patzig, J., Nave, K. A., and Werner, H. B. (2008). Phylogeny of proteolipid proteins: Divergence, constraints, and the evolution of novel functions in myelination and neuroprotection. *Neuron Glia Biol.* 4, 111–127. doi: 10.1017/S1740925X0900009X

Morell, P., Greenfield, S., Costantino-Ceccarini, E., and Wisniewski, H. (1972). Changes in the protein composition of mouse brain myelin during development. *J. Neurochem.* 19, 2545–2554. doi: 10.1111/j.1471-4159.1972.tb01313.x

Morell, P., Lipkind, R., and Greenfield, S. (1973). Protein composition of myelin from brain and spinal cord of several species. *Brain Res.* 58, 510–514. doi: 10.1016/0006-8993(73)90023-1

Morris, S. J., Louis, C. F., and Shooter, E. M. (1971). Separation of myelin proteins on two different polyacrylamide gel systems. *Neurobiology* 1, 64–67.

Musse, A. A., Gao, W., Homchaudhuri, L., Boggs, J. M., and Harauz, G. (2008). Myelin basic protein as a 'PI(4,5)P2-modulin': A new biological function for a major central nervous system protein. *Biochemistry* 47, 10372–10382. doi: 10.1021/bi801302b

Myllykoski, M., Eichel, M. A., Jung, R. B., Kelm, S., Werner, H. B., and Kursula, P. (2018). High-affinity heterotetramer formation between the large myelin-associated glycoprotein and the dynein light chain DYNLL1. *J. Neurochem.* 147, 764–783. doi: 10.1111/jnc.14598

Nasrabady, S. E., Rizvi, B., Goldman, J. E., and Brickman, A. M. (2018). White matter changes in Alzheimer's disease: a focus on myelin and oligodendrocytes. *Acta Neuropathol. Commun.* 6:22. doi: 10.1186/s40478-018-0515-3

Nave, K.-A., and Werner, H. B. (2014). Myelination of the Nervous System: Mechanisms and Functions. *Annu. Rev. Cell Dev. Biol.* 30, 503–533. doi: 10.1146/annurev-cellbio-100913-013101

Nawaz, S., Kippert, A., Saab, A. S., Werner, H. B., Lang, T., Nave, K. A., et al. (2009). Phosphatidylinositol 4,5-bisphosphate-dependent interaction of myelin basic protein with the plasma membrane in oligodendroglial cells and its rapid perturbation by elevated calcium. *J. Neurosci.* 29, 4794–4807. doi: 10.1523/JNEUROSCI.3955-08.2009

Nawaz, S., Sánchez, P., Schmitt, S., Snaidero, N., Mitkovski, M., Velte, C., et al. (2015). Actin filament turnover drives leading edge growth during myelin sheath formation in the central nervous system. *Dev. Cell.* 34, 139–151. doi: 10.1016/j.devcel.2015.05.013

Nawaz, S., Schweitzer, J., Jahn, O., and Werner, H. B. (2013). Molecular evolution of myelin basic protein, an abundant structural myelin component. *Glia* 61, 1364–1377. doi: 10.1002/glia.22520

Neilson, K. A., Ali, N. A., Muralidharan, S., Mirzaei, M., Mariani, M., Assadourian, G., et al. (2011). Less label, more free: Approaches in label-free quantitative mass spectrometry. *Proteomics* 11, 535–553. doi: 10.1002/pmic.201000553

Nguyen, M. V. C., Felice, C. A., Du, F., Covey, M. V., Robinson, J. K., Mandel, G., et al. (2013). Oligodendrocyte lineage cells contribute unique features to rett syndrome neuropathology. *J. Neurosci.* 33, 18764–18774. doi: 10.1523/JNEUROSCI.2657-13.2013

Norton, W. T., and Poduslo, S. E. (1973a). Myelination in rat brain: changes in myelin composition during brain maturation. *J. Neurochem.* 21, 759–773. doi: 10.1111/j.1471-4159.1973.tb07520.x

Norton, W. T., and Poduslo, S. E. (1973b). Myelination in rat brain: method of myelin isolation. *J. Neurochem.* 21, 749–757. doi: 10.1111/j.1471-4159.1973.tb07519.x

Olmos-Serrano, J. L., Kang, H. J., Tyler, W. A., Silbereis, J. C., Cheng, F., Zhu, Y., et al. (2016). Down syndrome developmental brain transcriptome reveals defective oligodendrocyte differentiation and myelination. *Neuron* 89, 1208–1222. doi: 10.1016/j.neuron.2016.01.042

Ott, C., Martens, H., Hassouna, I., Oliveira, B., Erck, C., Zafeiriou, M. P., et al. (2015). Widespread expression of erythropoietin receptor in brain and its induction by injury. *Mol. Med.* 21, 803–815. doi: 10.2119/molmed.2015.00192

Patzig, J., Erwig, M. S., Tenzer, S., Kusch, K., Dibaj, P., Möbius, W., et al. (2016). Septin/anillin filaments scaffold central nervous system myelin to accelerate nerve conduction. *eLife* 5:e17119. doi: 10.7554/eLife.17119.001

Perez-Riverol, Y., Csordas, A., Bai, J., Bernal-Llinares, M., Hewapathirana, S., Kundu, D. J., et al. (2019). The PRIDE database and related tools and resources in 2019: Improving support for quantification data. *Nucleic Acids Res.* 47, D442–D450. doi: 10.1093/nar/gky1106

Poitelon, Y., Kopec, A. M., and Belin, S. (2020). Myelin fat facts: an overview of lipids and fatty acid metabolism. *Cells* 9:812. doi: 10.3390/cells9040812

Quarles, R. H. (2007). Myelin-associated glycoprotein (MAG): Past, present and beyond. *J. Neurochem.* 100, 1431–1448. doi: 10.1111/j.1471-4159.2006.04319.x

Raasakka, A., Ruskamo, S., Kowal, J., Barker, R., Baumann, A., Martel, A., et al. (2017). Membrane association landscape of myelin basic protein portrays formation of the myelin major dense line. *Sci. Rep.* 7:4974. doi: 10.1038/s41598-017-05364-3

Roach, A., Takahashi, N., Pravtcheva, D., Ruddle, F., and Hood, L. (1985). Chromosomal mapping of mouse myelin basic protein gene and structure and transcription of the partially deleted gene in shiverer mutant mice. *Cell* 42, 149–155. doi: 10.1016/S0092-8674(85)80110-0

Roth, A. D., Ivanova, A., and Colman, D. R. (2006). New observations on the compact myelin proteome. *Neuron Glia Biol.* 2, 15–21. doi: 10.1017/S1740925X06000068

Saher, G., Brügger, B., Lappe-Siefke, C., Möbius, W., Tozawa, R. I., Wehr, M. C., et al. (2005). High cholesterol level is essential for myelin membrane growth. *Nat. Neurosci.* 8, 468–475. doi: 10.1038/nn1426

Saugier-Veber, P., Munnich, A., Bonneau, D., Rozet, J. M., le Merrer, M., Gil, R., et al. (1994). X-linked spastic paraplegia and Pelizaeus-Merzbacher disease are allelic disorders at the proteolipid protein locus. *Nat. Genet.* 6, 257–262. doi: 10.1038/ng0394-257

Schaeren-Wiemers, N., Bonnet, A., Erb, M., Erne, B., Bartsch, U., Kern, F., et al. (2004). The raft-associated protein MAL is required for maintenance of proper axon–glia interactions in the central nervous system. *J. Cell Biol.* 166, 731–742. doi: 10.1083/jcb.200406092

Schardt, A., Brinkmann, B. G., Mitkovski, M., Sereda, M. W., Werner, H. B., and Nave, K.-A. (2009). The SNARE protein SNAP-29 interacts with the GTPase Rab3A: implications for membrane trafficking in myelinating glia. *J. Neurosci. Res.* 87, 3465–3479. doi: 10.1002/jnr.22005

Schmidt, C., Hesse, D., Raabe, M., Urlaub, H., and Jahn, O. (2013). An automated in-gel digestion/iTRAQ-labeling workflow for robust quantification of gel-separated proteins. *Proteomics* 13, 1417–1422. doi: 10.1002/pmic.201200366

Schmitt, S., Cantuti Castelvetri, L., and Simons, M. (2015). Metabolism and functions of lipids in myelin. *Biochim. Biophys. Acta Mol. Cell Biol. Lipids.* 1851, 999–1005. doi: 10.1016/j.bbalip.2014.12.016

Sharma, K., Schmitt, S., Bergner, C. G., Tyanova, S., Kannaiyan, N., Manrique-Hoyos, N., et al. (2015). Cell type– and brain region–resolved mouse brain proteome. *Nat. Neurosci.* 18, 1819–1831. doi: 10.1038/nn.4160

Siems, S. B., Jahn, O., Eichel, M. A., Kannaiyan, N., Wu, L. M. N., Sherman, D. L., et al. (2020). Proteome profile of peripheral myelin in healthy mice and in a neuropathy model. *eLife* 9:e51406. doi: 10.7554/eLife.51406

Silva, J. C., Gorenstein, M. V., Li, G.-Z., Vissers, J. P. C., and Geromanos, S. J. (2006). Absolute Quantification of Proteins by LCMS E. *Mol. Cell. Proteomics* 5, 144–156. doi: 10.1074/mcp.M500230-MCP200

Simons, C., Wolf, N. I., McNeil, N., Caldovic, L., Devaney, J. M., Takanohashi, A., et al. (2013). A de novo mutation in the β-tubulin gene TUBB4A results in the leukoencephalopathy hypomyelination with atrophy of the basal ganglia and cerebellum. *Am. J. Hum. Genet.* 92, 767–773. doi: 10.1016/j.ajhg.2013.03.018

Simons, M., Krämer, E. M., Thiele, C., Stoffel, W., and Trotter, J. (2000). Assembly of myelin by association of proteolipid protein with cholesterol- and galactosylceramide-rich membrane domains. *J. Cell Biol.* 151, 143–154. doi: 10.1083/jcb.151.1.143

Snaidero, N., and Simons, M. (2017). The logistics of myelin biogenesis in the central nervous system. *Glia* 65, 1021–1031. doi: 10.1002/glia.23116

Snaidero, N., Velte, C., Myllykoski, M., Raasakka, A., Ignatev, A., Werner, H. B., et al. (2017). Antagonistic Functions of MBP and CNP establish cytosolic channels in CNS myelin. *Cell Rep.* 18, 314–323. doi: 10.1016/j.celrep.2016.12.053

Sommer, I., and Schachner, M. (1981). Monoclonal antibodies (O1 to O4) to oligodendrocyte cell surfaces: An immunocytological study in the central nervous system. *Dev. Biol.* 83, 311–327. doi: 10.1016/0012-1606(81)90477-2

Sprinkle, T. J., Sheedlo, H. J., Buxton, T. B., and Rissing, J. P. (1983). Immunochemical Identification of 2', 3'-Cyclic Nucleotide 3'-Phosphodiesterase in Central and Peripheral Nervous System Myelin, the Wolfgram Protein Fraction, and Bovine Oligodendrocytes. *J. Neurochem.* 41, 1664–1671. doi: 10.1111/j.1471-4159.1983.tb00878.x

Stuart, T., Butler, A., Hoffman, P., Hafemeister, C., Papalexi, E., Mauck, W. M., et al. (2019). Comprehensive integration of single-cell data. *Cell* 177:1888-1902.e21. doi: 10.1016/j.cell.2019.05.031

Taylor, C. M., Marta, C. B., Claycomb, R. J., Han, D. K., Rasband, M. N., Coetzee, T., et al. (2004). Proteomic mapping provides powerful insights into functional myelin biology. *Proc. Natl. Acad. Sci. U.S.A.* 101, 4643–4648. doi: 10.1073/pnas.0400922101

Thakurela, S., Garding, A., Jung, R. B., Müller, C., Goebbels, S., White, R., et al. (2016). The transcriptome of mouse central nervous system myelin. *Sci. Rep.* 6:25828. doi: 10.1038/srep25828

van der Knaap, M. S., Schiffmann, R., Mochel, F., and Wolf, N. I. (2019). Diagnosis, prognosis, and treatment of leukodystrophies. *Lancet Neurol.* 18, 962–972. doi: 10.1016/S1474-4422(19)30143-7

Vanrobaeys, F., Van Coster, R., Dhondt, G., Devreese, B., and Van Beeumen, J. (2005). Profiling of myelin proteins by 2D-gel electrophoresis and multidimensional liquid chromatography coupled to MALDI TOF-TOF mass spectrometry. *J. Proteome Res.* 4, 2283–2293. doi: 10.1021/pr050205c

von Büdingen, H. C., Mei, F., Greenfield, A., Jahn, S., Shen, Y. A. A., Reid, H. H., et al. (2015). The myelin oligodendrocyte glycoprotein directly binds nerve growth factor to modulate central axon circuitry. *J. Cell Biol.* 210, 891–898. doi: 10.1083/jcb.201504106

Wang, K. C., Koprivica, V., Kim, J. A., Sivasankaran, R., Guo, Y., Neve, R. L., et al. (2002). Oligodendrocyte-myelin glycoprotein is a Nogo receptor ligand that inhibits neurite outgrowth. *Nature* 417, 941–944. doi: 10.1038/nature00867

Werner, H. B., Krämer-Albers, E. M., Strenzke, N., Saher, G., Tenzer, S., Ohno-Iwashita, Y., et al. (2013). A critical role for the cholesterol-associated proteolipids PLP and M6B in myelination of the central nervous system. *Glia* 61, 567–586. doi: 10.1002/glia.22456

Werner, H. B., Kuhlmann, K., Shen, S., Uecker, M., Schardt, A., Dimova, K., et al. (2007). Proteolipid Protein Is Required for Transport of Sirtuin 2 into CNS Myelin. *J. Neurosci.* 27, 7717–7730. doi: 10.1523/JNEUROSCI.1254-07.2007

Yan, H., Helman, G., Murthy, S. E., Ji, H., Crawford, J., Kubisiak, T., et al. (2019). Heterozygous Variants in the Mechanosensitive Ion Channel TMEM63A Result in Transient Hypomyelination during Infancy. *Am. J. Hum. Genet.* 105, 996–1004. doi: 10.1016/j.ajhg.2019.09.011

Yang, H. J., Vainshtein, A., Maik-Rachline, G., and Peles, E. (2016). G protein-coupled receptor 37 is a negative regulator of oligodendrocyte differentiation and myelination. *Nat. Commun.* 7:10884. doi: 10.1038/ncomms10884

Yool, D. A., Klugmann, M., McLaughlin, M., Vouyiouklis, D. A., Dimou, L., Barrie, J. A., et al. (2001). Myelin proteolipid proteins promote the interaction of oligodendrocytes and axons. *J. Neurosci. Res.* 63, 151–164. doi: 10.1002/1097-4547(20010115)63:2<151::AID-JNR1007>3.0.CO;2-Y

Zeisel, A., Muñoz-Manchado, A. B., Codeluppi, S., Lönnerberg, P., Manno, G. L., Juréus, A., et al. (2015). Cell types in the mouse cortex and hippocampus revealed by single-cell RNA-seq. *Science* 347, 1138–1142. doi: 10.1126/science.aaa1934

Zhang, Y., Chen, K., Sloan, S. A., Bennett, M. L., Scholze, A. R., O'Keeffe, S., et al. (2014). An RNA-Sequencing Transcriptome and Splicing Database of Glia, Neurons, and Vascular Cells of the Cerebral Cortex. *J. Neurosci.* 34, 11929–11947. doi: 10.1523/JNEUROSCI.1860-14.2014

Zuchero, J. B., Fu, M. M., Sloan, S. A., Ibrahim, A., Olson, A., Zaremba, A., et al. (2015). CNS myelin wrapping is driven by actin disassembly. *Dev. Cell.* 34, 152–167. doi: 10.1016/j.devcel.2015.06.011